nature physics
SUPPLEMENTARY INFORMATION
DOI: 10.1038/NPHYS3030

Erasing no-man's land by thermodynamically stabilizing the liquid–liquid transition in tetrahedral particles

Frank Smallenburg
Department of Physics, Sapienza, Università di Roma, Piazzale Aldo Moro 2, I-00185, Roma, Italy.
Correspondence should be addressed to F. Smallenburg: (f smallenburg@gmail com).

Laura Filion
Soft Condensed Matter and Biophysics, Debye Institute for Nanomaterials Science, Utrecht University, Princetonplein 5, Utrecht, 3584 CC, the Netherlands.

Francesco Sciortino
Department of Physics, Sapienza, Università di Roma, Piazzale Aldo Moro 2, I-00185, Roma, Italy.

EFFECTS OF THE LIQUID-LIQUID PHASE SEPARATION OUTSIDE THE COEXISTENCE REGION

Although definitive evidence of a liquid-liquid (LL) phase separation requires observation at temperatures at and below the LL critical point (LLCP), its presence affects the thermodynamic behaviour of the system even at higher temperatures. In particular, quantities diverging at the critical point exhibit loci of extrema which can be observed in a wide region of the phase diagram [1] and originate at the critical point. Examples are provided by the isothermal compressibility K_T and the isobaric heat capacity C_P. In the LLCP hypothesis, the density anomalies of water and other tetrahedral liquids, where the density of the liquid phase exhibits a maximum as a function of the temperature at constant pressure, has been related to the extrema in response functions emanating from the LLCP [2]. In Fig. S1, we draw the pressure-temperature ($P-T$) phase diagram of the system with $\cos\phi = 0.825$ and $L = 0.5\sigma$, where the LL phase transition is thermodynamically stable. We do observe a line of constant-pressure density maxima ρ_{max} that occurs at temperatures above the LLCP, as well as lines connecting the extrema in K_T and C_P. Qualitatively, the diagram bears a striking resemblence to the one determined for the ST2 model for water[2]. Consistent with thermodynamic requirements [3], the point at which $dP/dT\ _{\rho_{max}} = \infty$ is also a K_T extremum.

The slope of the LL coexistence line $P_{\rm coex}(T)$ is positive, while it is expected to be negative in ST2. Via the Clausius-Clapeyron equation, this slope can be directly related to the difference in entropy between the two coexisting phases:

$$\frac{{\rm d}P_{\rm coex}}{{\rm d}T} = \frac{\Delta S}{\Delta V}, \qquad (1)$$

where ΔS and ΔV are respectively the difference in entropy and volume between the two phases. The positive slope indicates that the entropy of the high-density liquid (HDL) is lower than that of the low-density liquid (LDL). We also note that by construction, in this model, at low T both phases are fully bonded and hence have the same energy, imposing a vanishing coexisting pressure for $T \to 0$. Possibly, the slope of the coexistence curve, expecially close to the critical point, can be modulated by imposing a repulsive term disfavouring the denser phase and/or modulating the angular profile of the potential modeling the bond. Indeed in earlier work, it has been shown that increasing the bond directionality of a tetrahedral Kern-Frenkel-based potential, by combining a weaker flexible patch with a stronger narrow patch, can switch the slope of the Widom line (the line of maxima in C_P) from positive to negative [4]. Interestingly, in our case the slope of the coexistence line already decreases close to the critical point, and the Widom line, typically seen as the extension of the coexistence line, already shows a negative slope, suggesting that a minor modification to the model may be sufficient to match this aspect of the ST2 water phase diagram.

POTENTIAL ENERGY IN THE FLUID

Fig. S2 shows the behaviour of the potential energy U as a function of density for several different bond flexibilities ($\cos\phi$) and temperatures (T), at fixed $L = 0.5\sigma$. The system exhibits a clear minimum in the potential energy at an "optimal" network density [5], a characteristic of network-forming fluids. The minimum originates from the typical monotonic decrease of U with density at low ρ and from the breaking of the bonds associated with the progressive distortion of the tetrahedral geometry on increasing ρ beyond the optimal value. Counterintuitively, the minimum becomes deeper for less flexible bonds (higher $\cos\phi$). Although one might expect that making the bonds more directional would lead to a lower number of bonds in the system, the larger entropy of network states with broken bonds for wide angles leads to a larger U when $\cos\phi$ is large. Additionally, less flexible bonds also lead to more strongly structured tetrahedral networks [6], which may favor bond formation.

© 2014 Macmillan Publishers Limited. All rights reserved.

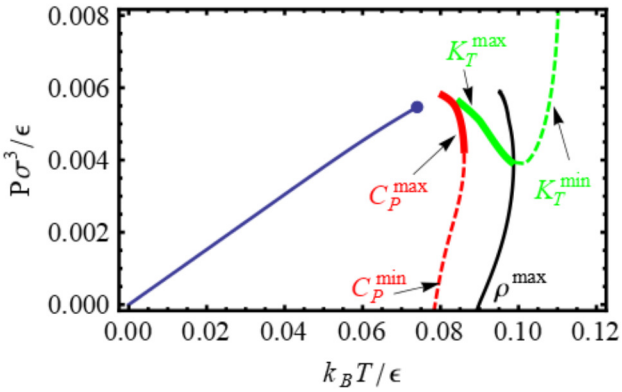

FIG. S1: Phase diagram of the tetramer model with $\cos\phi = 0.825$ and $L = 0.5\sigma$ in the $P-T$ plane. The blue line shows the LL coexistence line, ending in a critical point. The black line denotes the line of density maxima, where $\left(\frac{\partial\rho}{\partial T}\right)_P = 0$. The green line connects extrema in the isothermal compressibility K_T, i.e. points where $\left(\frac{\partial K_T}{\partial T}\right)_P = 0$, with the thicker solid line indicating maxima and the dashed line indicating minima. Similarly, the red line traces the extrema in the isobaric heat capacity C_P, i.e. where $\left(\frac{\partial C_P}{\partial P}\right)_T = 0$.

A secondary minimum could be expected at a density approximately a factor of two larger than the optimal density, indicating the possible formation of an interpenetrated network. Between these two densities, U shows a region of negative curvature, indicating an energetic driving force favoring phase separation [7].

Figure S3 shows U as a function of the reduced density $\rho^* = \rho(\sigma + L + \delta/2)^3$ for three different values of the softness. As expected, increasing the length of the arms leads to an overall lower number of bonds in the system. Additionally, the increase in energy when compressing the liquid beyond its optimal density is much less pronounced for small L, which is consistent with the fact that the LL phase transition disappears for sufficiently small L.

Finally, Fig. S4 shows the effects of $\cos\phi$ and L on the potential energy at fixed T.

COMMON TANGENTS

Figure S5 shows the common tangent constructions at temperature $k_BT/\epsilon = 0$ (with k_B Boltzmann's constant) for three different values of the bond flexibility at fixed softness $L = 0.5\sigma$.

HISTOGRAMS

To determine phase coexistences between the various fluid phases, we use both successive umbrella sampling (SUS) simulations (in the grand canonical ensamble) and

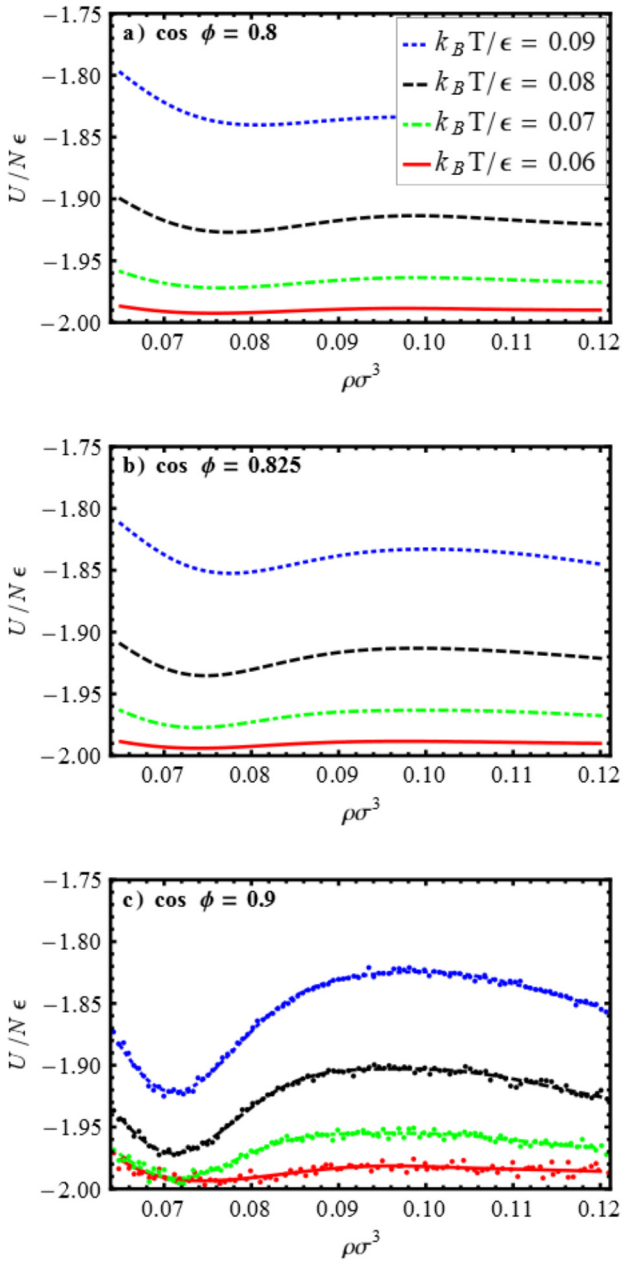

FIG. S2: Potential energy U per particle as a function of the density ρ at fixed $L = 0.5\sigma$, for three different values of the bond flexibility $\cos\phi$ and a range of temperatures, as indicated. In each plot, the set of temperatures shown is the same. The lines are fits to data from Monte Carlo simulations. In panel (c), the raw simulation data is also shown as points.

free-energy calculations, as explained in the Methods section. When using the SUS simulations, we evaluate the histogram $P(N)$, the probability to find N particles in the simulation box at fixed T, volume V and chemical potential μ. The histogram can be reweighted analytically by changing μ. In case of a coexistence, $P(N)$ must show two peaks of equal area, centered around the coexistence densities. If a coexistence is absent, only a single

© 2014 Macmillan Publishers Limited. All rights reserved.

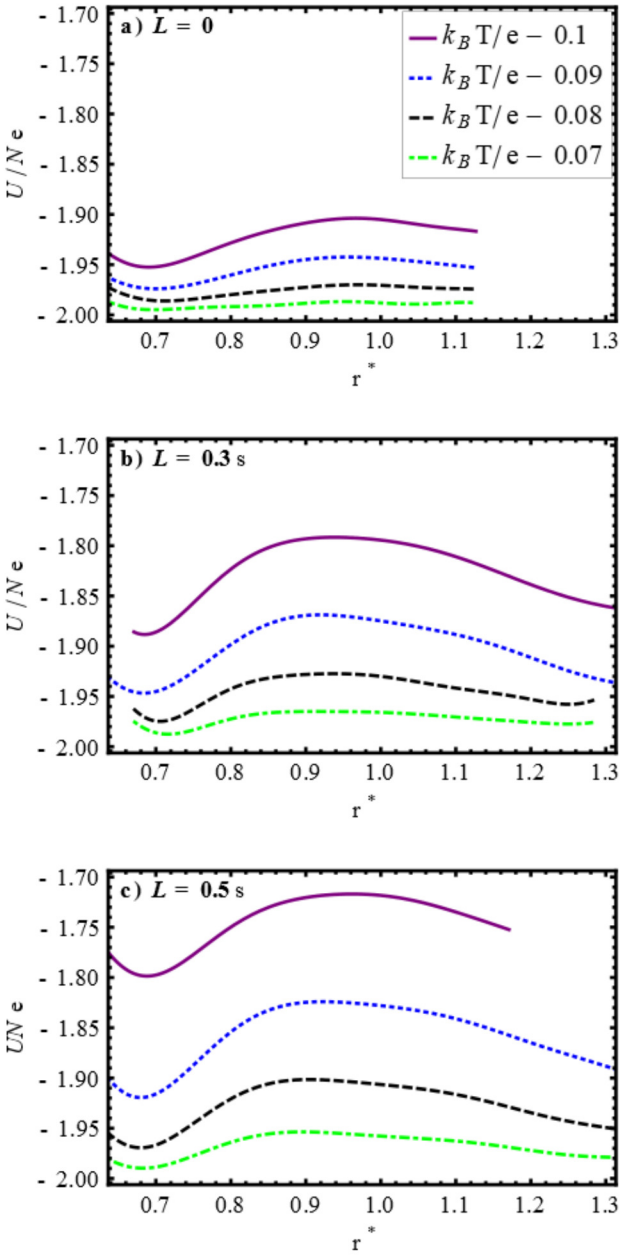

FIG. S3: Potential energy U per particle as a function of the density ρ at fixed $\cos\phi = 0.9$, for three different values of the softness L and a range of temperatures, as indicated. In each plot, the set of temperatures shown is the same. The lines are fits to data from Monte Carlo simulations. Note that panel (c) is partly based on the same data as Fig. S2c.

peak is observed. At low temperatures, the SUS simulations become difficult to equilibrate, and we resort to thermodynamic integration to determine the coexistence densities instead. To obtain the Helmholtz free energy per particle ($f = F/N$) as a function of T, we use:

$$\beta_2 f(\rho, T_2) = \beta_1 f(\rho, T_{\rm ref}) + \int_{\beta_{\rm ref}}^{\beta_2} {\rm d}\beta\, u(\rho, T), \quad (2)$$

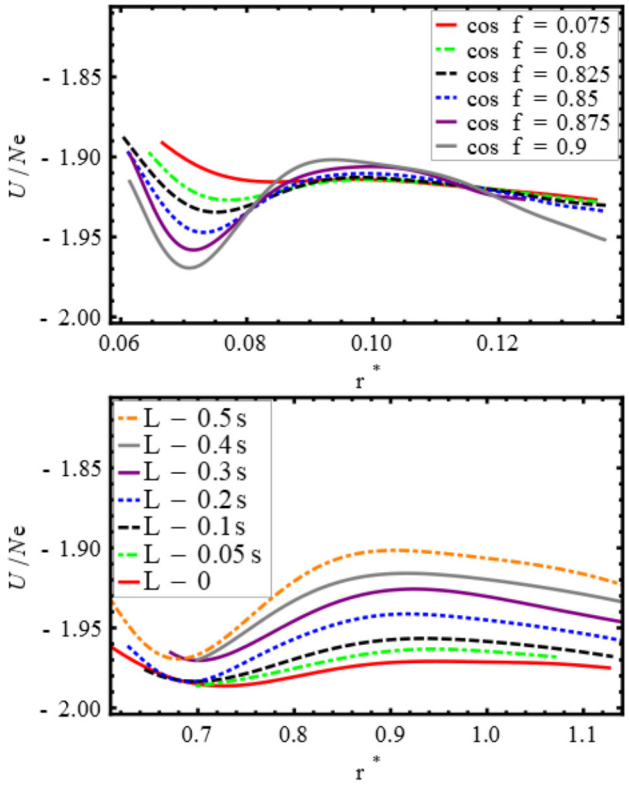

FIG. S4: Top: potential energy as a function of density at fixed arm length $L = 0.5\sigma$ and temperature $k_BT/\epsilon = 0.08$, for different values of the bond flexibility $\cos\phi$. Bottom: potential energy as a function of density at fixed bond flexibility $\cos\phi = 0.9$ and temperature $k_BT/\epsilon = 0.08$, for different values of the arm length L. The lines are fits to the simulation data.

where $u(\rho, T)$ the average potential energy per particle of the system at a given density and temperature, and $\beta = 1/k_BT$.

To calculate a reference Helmholtz free energy at high temperature $T_{\rm ref}$, we perform another run of SUS simulations, evaluating the chemical potentials in each of the SUS windows $\mu_{N,N+1}$ as

$$\beta\mu_{N,N+1} = \beta\mu - \log\left[\frac{P(N+1)}{P(N)}\right],$$

with μ the chemical potential used in the grand-canonical SUS simulation, and $P(N)$ the probability of observing N particles in the simulation. We also perform an NPT simulation at the same $T_{\rm ref}$ and intermediate density. We then combine the pressure P of the NPT simulation with $\mu_{N,N+1}$ obtained from the SUS simulation at the same density ($\rho_{\rm ref}$) to obtain a free energy

$$f_{\rm ref} = \mu - P/\rho_{\rm ref}. \quad (3)$$

Next, we use $\mu_{N,N+1}$ from all SUS windows to evaluate the free energy at $T_{\rm ref}$ for different numbers of particles

© 2014 Macmillan Publishers Limited. All rights reserved.

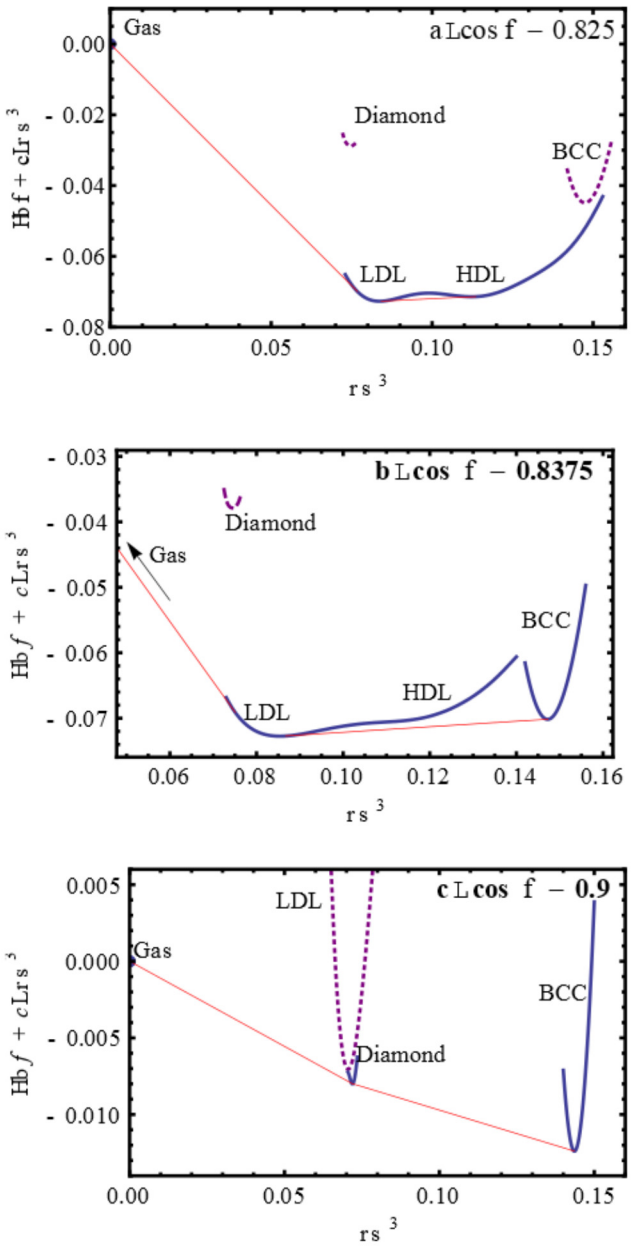

FIG. S5: Common tangent plots at $k_BT/\epsilon = 0$ for three of the phase diagrams in the Fig. 4 of the main text. The thick lines indicate the free energy per unit volume of the different phases. At each density, the phase or linear combination of two phases with the lowest free energy is stable. A constant linear term ($c\rho\sigma^3$) has been added in each plot to enhance readability; this has no effect on the resulting phase behaviour. Metastable phases are shown as dotted lines. The thinner red lines show the common tangent constructions connecting coexisting state points.

N in the same volume:

$$F(N,V,T) = Nf_{\rm ref} + \int_{N_{\rm ref}}^{N} \mu_{N,N+1}\,{\rm d}N, \qquad (4)$$

where $N_{\rm ref} = V\rho_{\rm ref}$ is the number of particles in the system at the reference density. We then evaluate, for each desired density, the free energy at other T using Eq. 2. Finally, to calculate a histogram from this free energy, we use:

$$P(N) / \exp(\beta\mu N)\exp(\beta F(N,V,T)), \qquad (5)$$

where μ is again tuned such that the two peaks have equal area, and the volume is chosen to match the one used in the SUS simulations.

Figure S6 shows examples of histograms at $\cos\phi = 0.9$ as obtained from SUS simulations, and histograms calculated (at the same volume $V = 1728\sigma^3$) from the free energies obtained via thermodynamic integration over the temperature. While the SUS data shows more noise, the coexistence densities from both methods agree very well.

Figure S6-(c) shows SUS histograms for both the gas-liquid and the LL transition for $\cos\phi = 0.9$ and $k_BT/\epsilon = 0.08$ and $k_BT/\epsilon = 0.09$. Note that the liquid coexisting with the gas and the low density liquid coexisting with the high density liquid have different densities. The chemical potentials of the two transitions are distinct as well: for $k_BT/\epsilon = 0.08$, $\beta\mu_{\rm GL} = -12.87$ and $\beta\mu_{\rm LL} = -11.16$, and for $k_BT/\epsilon = 0.09$, $\beta\mu_{\rm GL} = -10.03$ and $\beta\mu_{\rm LL} = -8.64$.

A second set of histograms, again at $V = 1728\sigma^3$, are shown in Fig. S7, for $\cos\phi = 0.825$. Interestingly, the valley between the two phases is not very deep even at $T = 0$. In other words, it is still easy for the system to switch between the two phases. Note that critical points are estimated by examining at which T the two peaks in the $P(N)$ histogram were twice as high as the valley between them [8].

EFFECT OF SYSTEM SIZE

To ensure that the phase transition is not an artifact of our small system size, we performed additional SUS simulations for larger system sizes, with a volume up to eight times larger than the standard one. In particular, we have investigated volumes up to $V = 13824\sigma^3$ for $L = 0.5\sigma$ and $\cos\phi = 0.9$. The LL critical point is clearly present for all explored system sizes, confirming the independence on system size of the critical phenomena. The histograms for several T for the largest system size investigated, calculated implementing histogram reweighting, are shown in Fig. S8.

COMPARING THE MODEL TO WATER

Qualitatively, the structure of liquid water at low temperatures is similar to that of tetravalent patchy particles with strong bond rigidity [6]. Thus, despite the simplicity of our model, it is instructive to consider mapping the tetramer model introduced here onto water. To do this,

© 2014 Macmillan Publishers Limited. All rights reserved.

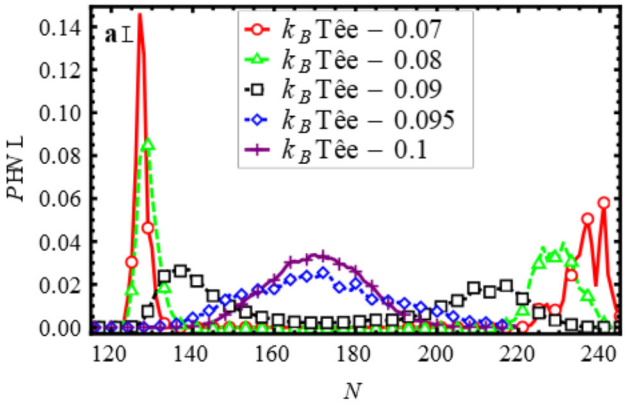

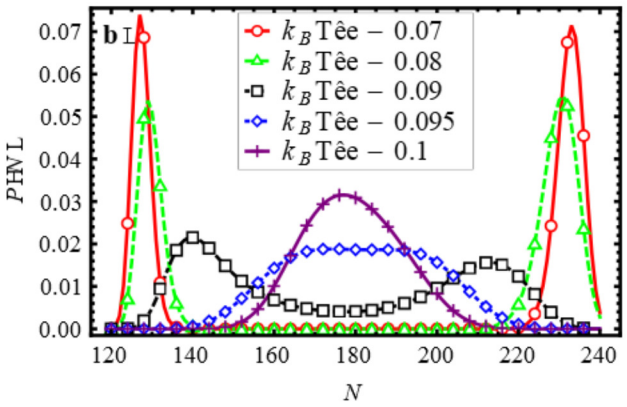

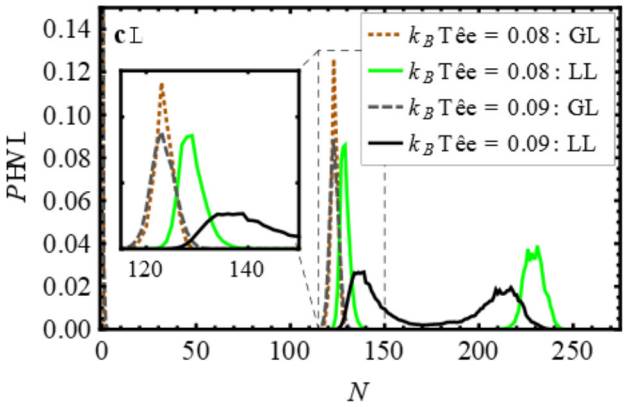

FIG. S6: Histograms obtained from **a)** SUS simulations and **b)** free-energy calculations (middle), at $L = 0.5\sigma$, $\cos\phi = 0.9$, and a range of temperatures as indicated. Note that for readibility, only some of the points are denoted by symbols. In **c)** we replot two of the SUS histograms, and include the SUS histograms for the gas-liquid coexistences at the same temperature (but different chemical potential) to provide evidence that the liquid coexisting with the gas and the low density liquid coexisting with the high density liquid have different densities (as clarified in the inset, which shows a zoomed-in version of the region outlined by dashed lines). Note that the gas peaks are barely visible, being located at $N \approx 0$.

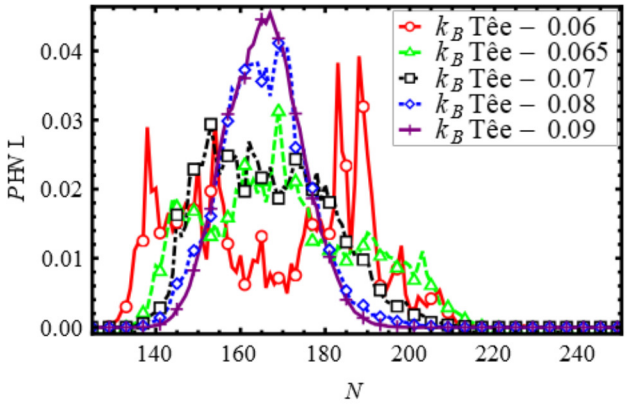

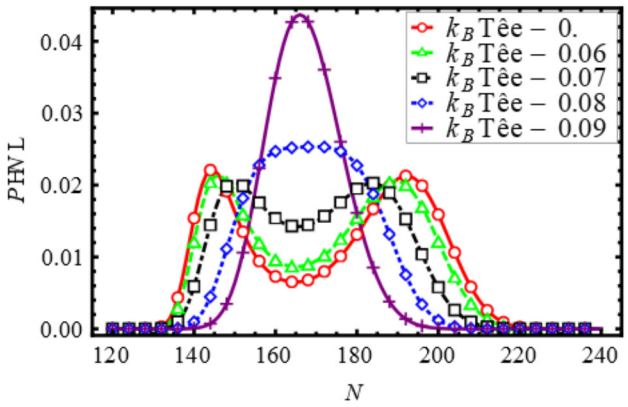

FIG. S7: Histograms obtained from SUS simulations (top) and free-energy calculations (bottom), at $L = 0.5\sigma$, $\cos\phi = 0.825$, and a range of temperatures as indicated. Note that for readibility, only some of the points are denoted by symbols.

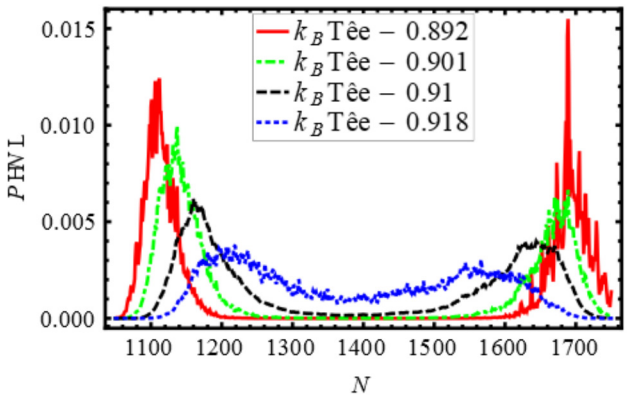

FIG. S8: Histograms obtained from SUS simulations for a large system size ($V = 13824\sigma^3$), at $L = 0.5\sigma$, $\cos\phi = 0.9$, and a range of temperatures as indicated.

we require an estimation of the bond flexibility $\cos\phi$ and bond length L.

From comparisons between the angular distribution and strength of the pre-peak of the structure factor between water and a standard Kern-Frenkel model, we can conclude that typical water models have a bonds

© 2014 Macmillan Publishers Limited. All rights reserved.

for which the directionality roughly corresponds to a patch opening angle of $\cos\theta \sqcap 0.95$ in the Kern-Frenkel model [6]. This is exactly the value of the opening angle $\cos\theta$ for bonding used in this article when no extra flexibility is added via $\cos\phi$. Thus, in terms of flexibility, the results for $\cos\phi = 1$ (region III in Fig. 3 of the main article) refer to the case of water.

Concerning L, we recall that this quantity controls the ratio between the distance of closest approach for unbonded (determined by σ) and bonded pairs (determined by $\sigma + L$) of particles. Analysis of the radial distribution function (and of its density dependence) can thus provide estimates of L for atomic and molecular systems. For the case of water, even when the density varies from $\rho = 0.92$ to $\rho = 1.4$ g/cm^3, there is no indication of pair of particles located at distances closer than the typical hydrogen bond distance: no signal shows up in the radial distribution function before the main peak [9]. Hence, one can conclude that water should be mapped into the case $L \,!\, 0$ and $\cos\phi \,!\, 1$. Consistent with experimental results, our calculations confirm that both for $L \,!\, 0$ and $\cos\phi \,!\, 1$ spontaneous crystallization prevails (Figs. 2 and 3 in the main text).

[1] Xu, L. et al. Relation between the widom line and the dynamic crossover in systems with a liquid–liquid phase transition. Proc. Natl. Acad. Sci. U.S.A. **102**, 16558–16562 (2005).

[2] Poole, P. H., Saika-Voivod, I. & Sciortino, F. Density minimum and liquid–liquid phase transition. J. Phys.: Condens. Matter **17**, L431 (2005).

[3] Sastry, S., Debenedetti, P. G., Sciortino, F. & Stanley, H. E. Singularity-free interpretation of the thermodynamics of supercooled water. Phys. Rev. E **53**, 6144 (1996).

[4] Tu, Y., Buldyrev, S. V., Liu, Z., Fang, H. & Stanley, H. E. Different water scenarios for a primitive model with two types of hydrogen bonds. Europhys. Lett. **97**, 56005 (2012).

[5] De Michele, C., Tartaglia, P. & Sciortino, F. Slow dynamics in a primitive tetrahedral network model. J. Chem. Phys. **125**, 204710 (2006).

[6] Saika-Voivod, I., Smallenburg, F. & Sciortino, F. Understanding tetrahedral liquids through patchy colloids. J. Chem. Phys. **139**, 234901 (2013).

[7] Poole, P. H., Sciortino, F., Essmann, U. & Stanley, H. E. Spinodal of liquid water. Phys. Rev. E **48**, 3799 (1993).

[8] Wilding, N. B. Critical-point and coexistence-curve properties of the lennard-jones fluid: a finite-size scaling study. Phys. Rev. E **52**, 602 (1995).

[9] Starr, F. W. et al. Thermodynamic and structural aspects of the potential energy surface of simulated water. Physical Review E **63**, 041201 (2001).

© 2014 Macmillan Publishers Limited. All rights reserved.